



THE UNIVERSITY *of* EDINBURGH

Edinburgh Research Explorer

A high-resolution and low-cost mesoscale tactile force sensor based on mode-localization effect and fabricated using rapid prototyping

Citation for published version:

Rehman, M-U, Saleem, MM, Tiwana, MI, Shakoor, RI & Cheung, R 2024, 'A high-resolution and low-cost mesoscale tactile force sensor based on mode-localization effect and fabricated using rapid prototyping', *Sensors and Actuators A: Physical*, vol. 369, 115140. <https://doi.org/10.1016/j.sna.2024.115140>

Digital Object Identifier (DOI):

[10.1016/j.sna.2024.115140](https://doi.org/10.1016/j.sna.2024.115140)

Link:

[Link to publication record in Edinburgh Research Explorer](#)

Document Version:

Peer reviewed version

Published In:

Sensors and Actuators A: Physical

General rights

Copyright for the publications made accessible via the Edinburgh Research Explorer is retained by the author(s) and / or other copyright owners and it is a condition of accessing these publications that users recognise and abide by the legal requirements associated with these rights.

Take down policy

The University of Edinburgh has made every reasonable effort to ensure that Edinburgh Research Explorer content complies with UK legislation. If you believe that the public display of this file breaches copyright please contact openaccess@ed.ac.uk providing details, and we will remove access to the work immediately and investigate your claim.



A High-Resolution and Low-Cost Mesoscale Tactile Force Sensor Based on Mode-Localization Effect and Fabricated Using Rapid Prototyping

Masood-Ur-Rehman^{a*}, Muhammad Mubasher Saleem^{a,b}, Mohsin Islam Tiwana^{a,b}, Rana Iqtidar Shakoor^c and Rebecca Cheung^d

^a Department of Mechatronics Engineering, National University of Sciences and Technology, Islamabad 44000, Pakistan

^b National Centre of Robotics and Automation (NCRA), Islamabad 44000, Pakistan

^c Department of Mechatronics Engineering, Air University, Islamabad 44000, Pakistan

^d Institute for Integrated Micro and Nano Systems, School of Engineering, University of Edinburgh, Scottish Microelectronics Centre, Edinburgh EH9 3FF, UK

* Correspondence: mrehman.mts20ceme@student.nust.edu.pk

Abstract

Keywords:

Capacitive sensing,
Electrostatic actuators,
High-resolution,
Low-cost,
Mesoscale,
Mode-localization,
Rapid prototyping,
Spring softening,
Tactile force sensor

This paper presents a novel design of a high resolution and low-cost tactile force sensor, based on the concept of mode-localization in two weakly coupled resonators (WCRs). The sensor is fabricated at mesoscale by utilizing rapid prototyping techniques. The two WCRs in the sensor are operated at resonance by using an electrostatic actuation. Change in the oscillation amplitude ratios and resonant frequency shift, corresponding to an input force is utilized as an output metric for the measurement of force. The application of an applied force on the WCRs induced electrostatic strain, which acted as a negative stiffness perturbation. The outer body of sensor is manufactured using a soft silicone elastomer and shaped using molds based on laser cutting technique. The proposed tactile force sensor is analyzed numerically through finite-element-method (FEM) based simulations. For the testing of tactile force sensor, an actuation and sensing electronics scheme is developed. The experimental results revealed that the sensor is capable of measuring input force up to 20 mN with a relative amplitude ratio (AR) and resonant frequency shift based sensitivity of 27040 ppm/mN and 3553 ppm/mN respectively. The experimentally evaluated resolution for the sensor is 7.3 μ N. The sensor shows the stability in response to the thermal variations and low-frequency vibrational environments.

1. Introduction

Robot assisted surgery is now preferred over conventional surgical procedures to access the internal human organs through small incisions with advantages of reduced recovery time for patient, minimized trauma, and reduced postoperative infections [1]. Despite the overwhelming performance of robotic surgical systems, one of the main limitations that persists is the absence of haptic feedback to surgical operators which may lead to exertion of excessive force by surgical tool leading to damage of the tissues and human organs [2]. To overcome this limitation, tactile sensors are generally integrated with surgical tool which measure the tool-tissue interaction (both kinesthetics and cutaneous) during the surgery. The tactile sensors are small scale devices which measure different properties of the contact between tool and body including contact force, roughness, texture, temperature, and shape. The tactile sensors that measure the contact force between the sensor and target object are termed as tactile force sensors [3]. The size of these sensors can vary from micrometers to millimeters depending on the application requirements. In terms of shape and size, tactile sensors can be classified into high spatial resolution based tactile sensing arrays, large-area tactile sensors, and single point contact tactile sensors [4]. For applications like measurement of tissue hardness and tissue palpation, the single point contact tactile force sensors offer advantages of small contact area for delicate tissues and requiring less calibration. Currently, several types

of tactile sensors have been proposed for different robotic surgery applications like measuring the hardness of soft tissues, force feedback for cardiovascular surgery, lump localization, tissue palpation, heart ablation, and vitreoretinal microsurgery [5]-[10]. These tactile sensors can be broadly classified based on two most commonly used transduction mechanisms i.e., optical and electrical. In optical tactile sensors, the basic sensing element is fiber optic. These sensors are further categorized into Fabry-Perot interferometers (FPI), Fiber-Bragg grating (FBG), and light intensity modulation (LIM) based sensors [11]. Optical tactile sensors are electrically passive and have high sensitivity and spatial resolution but are prone to signal distortion due to loss of light [12].

The electrical tactile sensors are based on electrical sensing element to characterize tool-tissue interaction. The sensing mechanisms of these tactile sensors are based on capacitive, piezoelectric, piezoresistive, magnetic, and inductive transduction [13]-[17]. These sensors can be further classified into stress-strain and resonance based tactile sensors to acquire spatial distribution of forces and tissue characterization in robotic surgery. The stress-strain based tactile sensors work on the principle of measuring static structural deformation for an applied input force. The tactile sensors based on stress-strain method have pros and cons which have been discussed in detail in [18], but the common limitation of these sensors is that their working requires deformation of tissue with an applied force,

which may cause damage to soft tissues due to an excessive force.

The frequency based tactile sensors termed as tactile resonance sensor or vibrotactile sensor use the spectral characteristics of a mechanical structure to measure the tactile perception. The resonant frequency of the mechanical structure moves, when sensor and tissue contacts with each other. These types of resonant sensors generally use piezoelectric ceramic material for actuation and sensing mechanism. The piezoelectric based tactile resonance sensors are used for the stiffness characterization in robotic surgery by measuring the resonant frequency shift of the system which consists of piezoelectric actuator, indenter head and tissue itself [19]-[21]. One of the drawbacks of these piezoelectric resonant tactile sensors include high resonant frequency of piezoelectric materials to which biological tissues does not show viscoelasticity that limits the scalability of such sensors [22].

MEMS technology based different resonant sensors, with high resolution and sensitivity, have been reported in the literature operating on the principle of the mode-localization in WCRs [23]-[32]. In mode-localization based sensors, small structural irregularity in identical WCRs causes vibrational energy confinement due to which both vibrational amplitude and resonant frequency of WCRs changes. Li et al. developed a mode-localization based novel electric current sensor based on two WCRs by using the silicon-based microfabrication process [24]. The sensor was able to measure the sub-microampere current. A computational investigation of high order mode localization is observed by Lyu et al. for electrostatically coupled weakly coupled microbeams [27]. The authors established reduced order model to analyse the effect of coupling strength, coupling mode, and actuation forces on the dynamics of the system. The authors theoretically observed that AR sensitivity is orders of magnitude higher than the frequency-based sensitivity for mass sensing. Zhao et al. developed electrostatic force sensor in 3 WCRs by using the microfabrication process [26]. To the best of authors knowledge, mode-localization based tactile force sensor has not been developed at any scale. MEMS based sensors discussed earlier are fabricated using a customized microfabrication process which requires high fabrication cost and long device development cycle [33]. One of the requirements of tactile sensor for robotic surgery is disposability of the sensor, because tactile sensor cannot be sterilized repeatedly [34]. In this paper, we report a low cost and high-resolution single point contact mesoscale soft resonant tactile force sensor by utilizing the concept of mode-localization in WCRs. The resonating structure is harmonically actuated using the electrostatic force and oscillation is sensed through the capacitive sensing mechanism. Theoretically predicted modes and resonant frequencies are validated through numerical as well as experimental procedures with an experimentally evaluated resolution of $0.53 \mu\text{N}$. The mode localization phenomenon, which was earlier investigated in MEMS sensors, is

successfully demonstrated for the proposed tactile force sensor fabricated using a low-cost rapid prototyping technique.

2. Sensor Design and Structural Dynamics

2.1. Working Principle

The proposed tactile force sensor is based on the mode localization in two WCRs under the influence of an input force. The sensor structure consists of two fixed-free cantilever beam resonators, with a square plate at the end, and having identical geometric shape and dimensions. One of the resonators, labeled as resonator 1 in Fig. 1(a), is electrostatically actuated at resonant frequency using an actuation electrode placed above resonator 1. The second resonator i.e., resonator 2 is mechanically coupled with resonator 1 and is located beneath a forcing cantilever. When an actuation voltage is applied to the resonator 1, both resonators start oscillating at the same resonant frequency with nearly the same oscillation amplitude. A sensing electrode is placed below each resonator to measure the oscillation amplitude of the resonators using a capacitive sensing mechanism. An external force on the top elastomer results in a mechanical deflection in the forcing cantilever which induces electrostatic strain causing negative stiffness perturbation in the resonator 2 due to spring softening phenomena. This electrostatic perturbation results in a shift in resonant frequency and oscillation amplitudes of both resonators. For the proposed sensor, the shift in the resonant frequency and AR of the WCRs can be used as an output to measure the external input force. Figure 1 (b) and (c) show the labelled dimensions and three-dimensional (3D) schematic of the assembled tactile force sensor respectively. The dimensions and parameters of the proposed design are specified in Table. I.

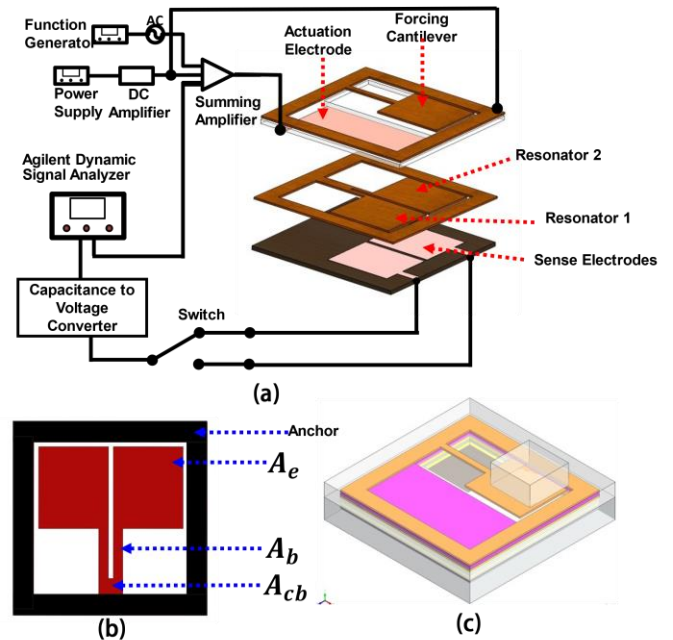


Fig. 1. (a) Exploded view of the force sensor. (b) Mechanical structure of the 2-DOF WCRs. (c) 3D model of the proposed tactile force sensor.

TABLE I: DESIGN PARAMETERS FOR THE PROPOSED TACTILE FORCE SENSOR.

Design Parameters	Values
Area of electrode (A_e)	$17 \times 14.5 \text{ mm}^2$
Area of beam (A_b)	$14 \times 2 \text{ mm}^2$
Area of coupling beam (A_{cb})	$4 \times 1 \text{ mm}^2$
Stiffness of forcing cantilever (k_f)	62.67 N/m
Stiffness of resonators (k)	26.42 N/m
Thickness of structure (t)	0.1 mm
Mass of resonators (m)	$1.974 \times 10^{-4} \text{ kg}$
Resonator 1 and actuation electrode gap (d_0)	1.5 mm
Resonator and sensing electrode gap (d_f)	1.5 mm
Resonator 2 and forcing electrode gap (d_2)	2.5 mm
Overall size of the sensor	$38 \times 38 \text{ mm}^2$

2.2. Dynamic Model of Weakly Coupled Resonators (WCRs)

The two weakly coupled mechanical resonators in the proposed tactile force sensor can be illustrated as a two degrees of freedom (2-DOF) spring-mass-damper model as shown in Fig. 2. As the resonators in WCRs are identical, effective mechanical stiffness, mass and damping coefficients of resonators are assumed to be equal, i.e., $k = k_1 = k_2$, $m = m_1 = m_2$ and, $c = c_1 = c_2$. The mechanical coupling between the two resonators is modeled by a coupling stiffness (k_c) and the electrostatic stiffness perturbation in the resonator 2 is considered as Δk . The resonators motion can be represented in the form of equations which can be written as;

$$m \ddot{x}_1 + c \dot{x}_1 + (k + k_c)x_1 - k_c x_2 = f_1 \quad (1)$$

$$m \ddot{x}_2 + c \dot{x}_2 - k_c x_1 + (k + k_c \pm \Delta k)x_2 = 0 \quad (2)$$

Equations (1) and (2) can be written in matrix form as;

$$\mathbf{M}\ddot{\mathbf{x}} + \mathbf{C}\dot{\mathbf{x}} + \mathbf{K}\mathbf{x} = \mathbf{F} \quad (3)$$

Where,

$$\mathbf{M} = \begin{bmatrix} m & 0 \\ 0 & m \end{bmatrix}, \quad \mathbf{C} = \begin{bmatrix} c & 0 \\ 0 & c \end{bmatrix}, \quad \mathbf{K} = \begin{bmatrix} k + k_c & -k_c \\ -k_c & k + k_c \pm \Delta k \end{bmatrix},$$

represents mass, damping, and stiffness matrix respectively,

while $\mathbf{F} = \begin{bmatrix} f_1 \\ 0 \end{bmatrix}$, $\mathbf{x} = \begin{bmatrix} x_1 \\ x_2 \end{bmatrix}$, are force and displacement matrix respectively. Assuming that there is no external force and effect of damping is negligible, the dynamic equations of motion are given as;

$$m \ddot{x}_1 + (k + k_c)x_1 - k_c x_2 = 0 \quad (4)$$

$$m \ddot{x}_2 - k_c x_1 + (k + k_c \pm \Delta k)x_2 = 0 \quad (5)$$

The general solution of equation (4) and (5) is in the form of;

$$\begin{bmatrix} x_1 \\ x_2 \end{bmatrix} = \begin{bmatrix} u_{0i} \\ u_{0i} \end{bmatrix} e^{j\omega_{0i}t} \quad (6)$$

Here, u_{0i} and ω_{0i} are the eigenvectors (amplitude ratio) and eigenvalue ($\lambda = \omega_{0i}^2$). Using equation (6), the expression for eigenvalue and eigenvector can be obtained as;

$$\omega_i^2 = \frac{2k - \Delta k + 2k_c \pm \sqrt{\Delta k^2 + 4k_c^2}}{2m}; \quad (7)$$

$$u_i = \frac{x_{2i}}{x_{1i}} = \frac{\Delta k \pm \sqrt{\Delta k^2 + 4k_c^2}}{2k} \quad (8)$$

Where i denotes mode number of the system. Initially, when

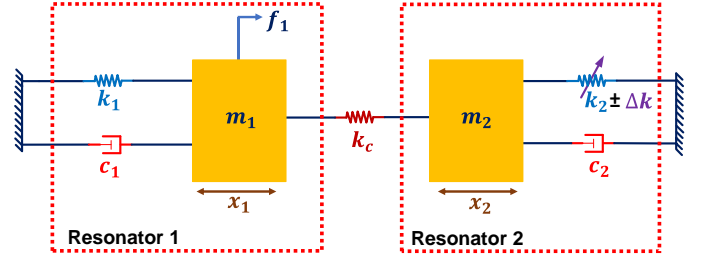


Fig. 2. Representation of 2-DOF WCRs in tactile force sensor as spring-mass-damper model.

stiffness perturbation (Δk) of the system is zero, AR and resonant frequency for first two modes are;

$$\omega_1 = \sqrt{\frac{k}{m}}, \quad \omega_2 = \sqrt{\frac{k+2k_c}{m}} \quad (9)$$

$$u_1 = 1, \quad u_2 = -1 \quad (10)$$

Equation (9) shows that when $k_c=0$, the two resonators are completely decoupled and only one mode exists for each resonator. When $k_c = k$, the two resonators are fully coupled and resonant frequency of second mode is 1.732 times higher than the first mode resonant frequency. So, the mechanical coupling between two resonators range from 0 to 1, which can be written as $0 < k_c/k < 1$. The factor $\kappa = k_c/k$ is called coupling factor which represents the coupling strength between the two resonators. Equation (10) shows that in the absence of external perturbation, the amplitude at resonance of WCRs is equal at first and second mode, however the two resonators move in-phase at first mode and out-of-phase at second mode.

By considering the effect of the normalized external perturbation ($\delta = \Delta k/k$) and coupling factor κ , the equations (7) and (8) can be written as;

$$\omega_i^2 = \left(1 - \kappa + \frac{1}{2}\delta \pm \sqrt{\delta^2 + 4\kappa^2}\right) \omega_0^2 \quad (11)$$

$$u_i = \frac{\delta \pm \sqrt{\delta^2 + 4\kappa^2}}{2\kappa} \quad (12)$$

Figure 3(a) shows that the oscillation amplitude of both resonators is equal with AR = (x_1/x_2) i.e., the oscillation amplitude of both resonators have ratio 1 at zero stiffness perturbation. For a positive value of δ , the AR value increases in first mode and decreases in second mode, while for the negative δ values an opposite behaviour occurs. The effect of change in the δ values on first and second mode resonant frequency is shown in Fig. 3(b). For positive δ values, the second resonant frequency increases linearly, while remains almost constant for the first resonant frequency.

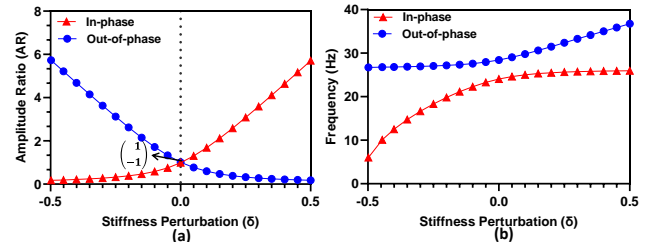


Fig. 3. Effect of the stiffness perturbation on (a) Amplitude ratio. (b) Resonant frequency of the 2-DOF WCRs.

On other hand, for the negative δ values, both first (in-phase) and second (out-of-phase) resonant frequency decreases. However, the decrease in the out-of-phase resonant frequency is very small in comparison to in-phase mode resonant frequency.

The resonant frequency shift and AR based sensitivity for the 2-DOF WCRs for any mode can be written in terms of coupling factor and stiffness perturbation and is given as;

$$S_F = \left| \frac{\omega_i - \omega_i^0}{\omega_i^0} \right| \approx \left| \frac{\Delta k}{2k} \right| = \left| \frac{\delta}{2} \right| \quad (13)$$

$$S_{AR} = \left| \frac{u_i - u_i^0}{u_i^0} \right| \approx \left| \frac{\Delta k}{4k_c} \right| = \left| \frac{\delta}{4\kappa} \right| \quad (14)$$

The equation (14) shows that the AR sensitivity is dependent on the coupling between the two resonators. From equation (9), it is evident that as the mechanical coupling between the two oscillating structures weakens, the separation between the mode resonant frequencies decreases when the external stiffness perturbation is absent. The equation (9), in terms of first and second mode resonant frequencies can be used to represent the mechanical coupling factor as;

$$\kappa = \frac{\omega_{op}^2 - \omega_{ip}^2}{2\omega_{ip}^2} \quad (15)$$

The above equation shows that at a certain low value of κ , both modes coincide with each other and are no more distinguishable. This phenomenon is termed as mode-aliasing. For the 2-DOF WCRs, the criteria that must be fulfilled to avoid mode-aliasing is given as $\omega_{op} - \omega_{ip} > \omega_{3dB}$, ($f_{op} - f_{ip} > f_{3dB}$) i.e. the frequency splitting between the two modes should be greater than the -3dB bandwidth of a mode to avoid mode-aliasing [29]. This condition limits the maximum AR sensitivity which is inversely proportional to the κ value.

2.3. Electrostatic Force as Stiffness Perturbation

The forcing cantilever and resonator 2 are designed in a parallel plate configuration as illustrated in Fig. 1(a). When a bias voltage is applied between these two, an electrostatic force is developed which is given by;

$$F_e = -\frac{\epsilon_0 AV^2}{2(d_2 - d)^2} \quad (16)$$

Where A is the overlapping area of two plates, ϵ_0 is permittivity, V is electric potential, d_2 is initial gap between the forcing cantilever and resonator 2, and d is the displacement due to an external mechanical force applied to the forcing cantilever. For a parallel plate configuration, the electrical spring constant due to an electrostatic force can be written as;

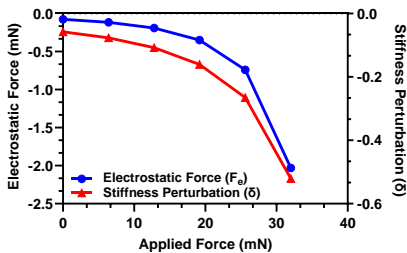


Fig. 4. Effect of applied force on electrostatic force between the forcing cantilever and resonator 2 and resultant stiffness perturbation.

$$k_e = -\frac{\epsilon_0 AV^2}{2(d_2 - d)^3} \quad (17)$$

By using equations (16) and (17), the normalized stiffness perturbation in resonator 2, corresponding to a displacement in the forcing cantilever under external force, can be written as;

$$\delta = \frac{\Delta k}{k} = -\frac{2\epsilon_0 AV^2 l^3}{Ewt^3(d_2 - d)^3} \quad (18)$$

Where w , t , l , and E are width, thickness, length, and Young's modulus of the resonator respectively. The results in Fig. 4 shows that for an applied force on the sensor, magnitude of the electrostatic force and corresponding negative stiffness perturbation in the resonator 2 increases linearly for small values of applied force i.e., up to 20 mN and nonlinearity increases as magnitude of applied force to the sensor increases.

3. Finite Element Method (FEM) Analysis

The proposed mode-localization based tactile force sensor is numerically simulated through FEM analysis by using the Comsol Multiphysics software and various characteristics of the sensor are obtained. In the FEM analysis, density of 8960 kg/m³, Young's modulus of 130 GPa, and Poisson's ratio of 0.35 are used for the resonating copper material [35]. The free tetrahedral mesh is generated for the tactile force sensor, which has maximum and minimum element size of 1.79 mm and 0.128 mm respectively. The sensor is mainly actuated through electrostatic force. Static or DC analysis of electrostatic force is conducted to obtain the feasibility of actuating the mechanical structure at meso-scale. Moreover, modal analysis of the structure is conducted to acquire mode shapes of the resonating structure. The mechanical structure is perturbed by applying an external force on forcing cantilever which reduces the gap between forcing cantilever and resonator 2 and induces electrostatic stiffness perturbation in the WCRs. Dynamic frequency response analysis and electrostatic force perturbation analysis are conducted to obtain the frequency shift and AR variation of the sensor.

3.1. Electrostatic Actuation Analysis

The resonator 1 of proposed sensor is set into oscillation by applying an electrostatic actuation voltage between the resonator 1 plate and top actuation electrode. To observe the impact of the applied actuation voltage (VDC) on displacement of the resonator and electrostatic force strength, a coupled electric field-mechanical analysis is carried out using the FEM simulation software. Figure 5 (a) shows effect of increase in the

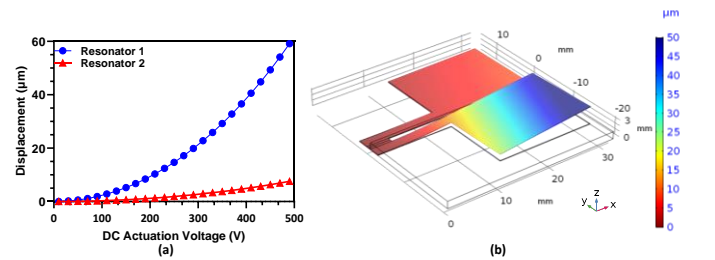


Fig. 5. (a) Effect of increase in DC actuation voltage applied to resonator 1 on displacement of the 2-DOF WCRs. (b) Displacement profile of the 2-DOF WCRs under an actuation voltage.

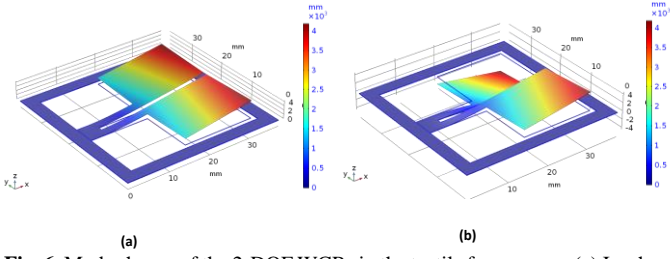


Fig. 6. Mode shapes of the 2-DOF WCRs in the tactile force sensor (a) In-phase mode at 20.8 Hz. (b) Out-of-phase mode at 24.6 Hz.

actuation voltage to the resonator 1 on displacement amplitudes of both resonators. The displacement of resonator 1 increases nonlinearly with an increase in the actuation voltage and air gap between the two electrodes decreases under electrostatic force. Resonator 2 is weakly coupled with resonator 1 which induces small displacement in resonator 2 because of mechanical coupling as shown in Fig 5(b). The maximum deflection in resonators is observed at the tip of resonators. The sensors based on the phenomenon of mode-localization, discussed in the literature are mostly fabricated using MEMS technology and one of the limitations for such sensors, for achieving high oscillation amplitude in coupled resonators, is the pull-in effect owing to air gaps in the range of micrometers between two micro-plates. However, since the air gap between the resonator 1 and actuation electrode for the proposed sensor is 1.5 mm and the displacement in the resonator plate is only $60 \mu\text{m}$ at 500 V, the pull-in effect does not occur up to 500 V.

3.2. Frequency Analysis of the 2-DOF WCRs in Sensor

The natural frequency response and related mode shapes of the 2-DOF WCRs is obtained using FEM simulations. The first resonance frequency value is 20.8 Hz and the oscillations of both resonators are in-phase as appeared in Fig. 6 (a). The second mode frequency lies at 24.6 Hz and at this frequency both the resonators oscillate in out-of-phase as shown in Fig. 6(b). The natural frequencies obtained for the WCRs are low due to the design of mesoscale cantilever resonators having square plate at the end of cantilever.

The air gap between 2-DOF WCRs and the sensing plates exerts damping force on the resonators. The energy loss in the resonators can be modeled in terms of Rayleigh damping by using a linear combination of stiffness and mass matrices given as [36];

$$2\xi_i = \frac{\alpha}{\omega_i} + \beta\omega_i \quad (19)$$

Where ξ_i and ω_i are the damping ratio and natural frequency, for $i = 1, 2$. The distribution of air pressure between the gap of two plates can be modeled using the effective air viscosity [37];

$$\eta_{eff} = \frac{\eta}{1 + 9.368k_n^{1.159}} \quad (20)$$

Where k_n is Knudson number, and η is the air viscosity coefficient. Knudson number is defined as the ratio of air molecule mean free path and air gap between plates. Using equation (20), the effective air viscosity for the parallel plate resonator in the proposed sensor at atmospheric pressure is

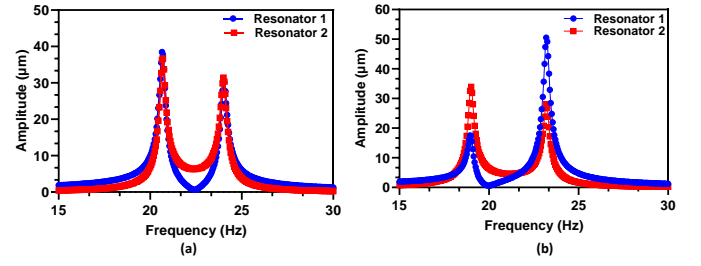


Fig. 7. Frequency response of the 2-DOF WCRs in the sensor, (a) at no input force. (b) at 20 mN input force.

$1.859e^{-5}$ Pa-s. The relation between the damping coefficients of a resonators and effective viscosity is given as;

$$c = \eta_{eff} \frac{A}{d_0} \quad (21)$$

Where d_0 and A is air gap between the resonators and sensing electrodes and overlap area respectively. The damping ratio ($\zeta = c/2m\omega_n$) for the 2-DOF WCRs is obtained using equation (21). The values of mass and stiffness matrix multiplier are calculated as $\alpha = 1.5$ Hz and $\beta = 2.32e^{-5}$ s for the natural frequency and damping ratio value of $\xi_1 = 0.0396$ and $\xi_2 = 0.032$. These values are included in the FEM simulation to model the air damping effect.

The force perturbation response is computed by applying an external force on the forcing electrode located above the resonator 2. The gap between two plates is set as 2.5 mm and 600 V is applied on the forcing cantilever. Resonator 1 is harmonically actuated using 50 V_{DC} and 50 V_{AC}. The dynamic frequency response of the WCRs, without applied force, is shown in Fig. 7(a). The first two modes resonant frequency values are 20.65 Hz and 23.9 Hz respectively. The mode frequency splitting (Δf) is the difference between out-of-phase mode and in-phase mode ($\Delta f = f_{op} - f_{ip}$) resonant frequencies. As discussed in section II (b), the mode frequency splitting should be higher than the f_{3dB} , which is the difference of two frequencies at 77% of vibrational amplitude to avoid mode aliasing condition. The modes frequency splitting (Δf) is 3.4 Hz which is greater than the f_{3dB} i.e., $\Delta f = 8.5f_{3dB}$. Thus, the mode-aliasing condition to prevent mode coincidence is satisfied for the 2-DOF WCRs at zero input force. The oscillation amplitudes of both resonators are approximately equal.

Figure 7(b) shows the dynamic frequency response of WCRs with an applied force of 20 mN. The resonant frequency and peak voltage of resonator 1 shifts due to the external perturbation force. The amplitude of the resonator 1 decreases

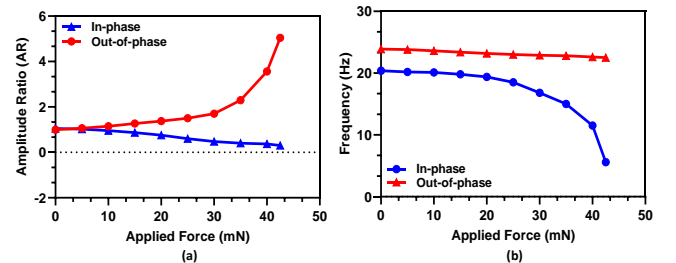


Fig. 8. The effect of increasing input force to the sensor on (a) AR and (b) frequency shift of the 2-DOF WCRs at both in-phase (first) and out-of-phase (second) mode.

from initial value of 38.48 μm to 18.7 μm at in-phase mode and increases from the initial value of 30.3 μm to 50.51 μm at the second mode. The amplitudes of resonator 2 decreases from the initial value of 36.68 μm to 32.1 μm and 31.45 μm to 27.04 μm at both first and second mode respectively.

Figure. 8(a) and (b) depict the AR (Ratio of the vibrational amplitudes of resonator-1 and resonator-2 at in-phase and out-of-phase modes), and frequency shift of the WCRs for an increasing applied force. The AR of the WCRs is approximately 1 at both modes when no external force is applied. With an increase in the applied force, the AR of 2-DOF WCRs decreases at first mode and increases at second mode. The change in the AR at second mode is higher in comparison to the first mode. This shows that for the proposed sensor the 2-DOF WCRs should be operated at out-of-phase mode frequency to achieve better sensitivity. The AR response at out-of-phase mode is linear with a coefficient of determination (R^2) value of 0.987 for 30 mN range and AR changes from 0.96 to 1.7 for this range. Figure 8(b) shows the shift in the first and second mode frequency with an increase in the external applied force. The results show that the shift in the second mode frequency with an external applied force is negligible to 40 mN. However, the first mode frequency decreases with an increase in the external applied force. The shift in the first mode frequency is more dominant for an applied force above 20 mN. This can be attributed to the non-linear behavior of the stiffness perturbation due to electrostatic force.

4. Experimental Setup

4.1. Sensor Fabrication and Experimental Setup

The mode-localization based tactile force sensor is fabricated using the conventional machining process. Size of the sensor is 38 mm \times 38 mm \times 8 mm, and it comprises eight parts as illustrated in Fig. 9(a). The outer body of sensor is fabricated using a soft silicone elastomer (Ecoflex 00-30) and

shaped using molds. The molds for silicone elastomers are developed by laser cutting the polymethyl methacrylate (PMMA) sheet of 1 mm thickness. The WCRs and forcing electrode of sensor are fabricated using copper metal. The mechanical structure is precisely cut through wire electrical discharge machining (WEDM) process. The actuation and oscillation sensing electrodes at the top and bottom of the tactile sensor are fabricated on a printed circuit board (PCB). The PCB for actuation electrode and forcing electrode is covered with insulating material to prevent short-circuit with resonating structures. The gap between electrodes and resonator is maintained using parts which are cut from inside area where mechanical resonators vibrate. These parts are fabricated using PMMA sheet of 1.5 mm thickness and machined by a laser machining process. The air gap between the resonator 1 and actuation electrode is set as 1.5 mm, while gap between resonator 2 and forcing electrode is 2.5 mm. The total fabrication and assembling cost of the sensor, with electronics component is around US\$ 20.

The fabricated tactile force sensor is tested by applying a mechanical force on the top side of the sensor where forcing cantilever is located. The test setup for the device is shown in Fig. 9(b). The tactile force sensor is placed on a 3-axis position stage. The applied force is measured from force gauge. The analog force gauge can measure the applied force by placing the force gauge needle perpendicular to the object. However, for single point contact force measurement, the force gauge needle is inclined at 32 degrees. The measured force and applied force are not equal due to an inclined angle, leading to the relationship of $F_{measured} = 0.848 \times F_{applied}$. The position of the force gauge is precisely controlled by using a stepper motor which can produce 0.1 mm displacement for each step in the vertical direction. The actuation and sensing electronics are biased from a power supply of ± 15 V. The oscillation amplitude of the resonators is measured through sensing electronics circuit. The actuation voltage can be either applied to the resonator 1 through a function generator to observe the oscillation amplitude of resonators in time domain at a single frequency or through a dynamic signal analyzer (Agilent 35670A) which can be used to obtain frequency response of the resonators. The dynamic signal analyzer (DSA) is used to apply a sinusoidal sweep and obtain the frequency response of the resonators. By considering the applied force, AR and resonant frequency shift are then calculated for the 2-DOF WCRs in the tactile force sensor.

4.2. Signal Processing Electronics

The mechanical structure of the tactile force sensor is harmonically actuated using an AC voltage superimposed on DC voltage. The signal provides electrostatic force to move the resonator 1 sinusoidally. The harmonic signal is obtained from the electronics circuit specifically designed for the actuation of the sensor. The motion of each resonator is sensed through sense electronics. The schematic of the actuation and sensing electronics integrated with the sensor is shown in Fig. 10. As shown in the figure, the actuation electrodes of tactile force sensor are connected to the output of actuation electronics, and sense electrodes are connected to the input of

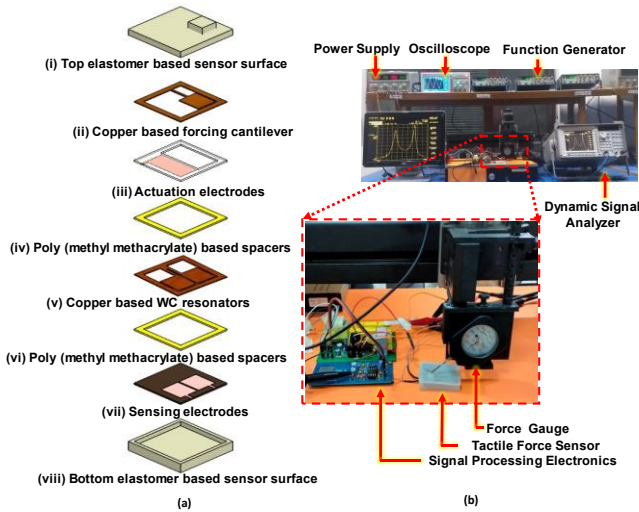


Fig. 9. (a) An exploded view of the tactile force sensor showing its eight individual parts. Part (i) is positioned at the top and part (viii) is positioned at the bottom of assembled sensor. (b) Experimental setup.

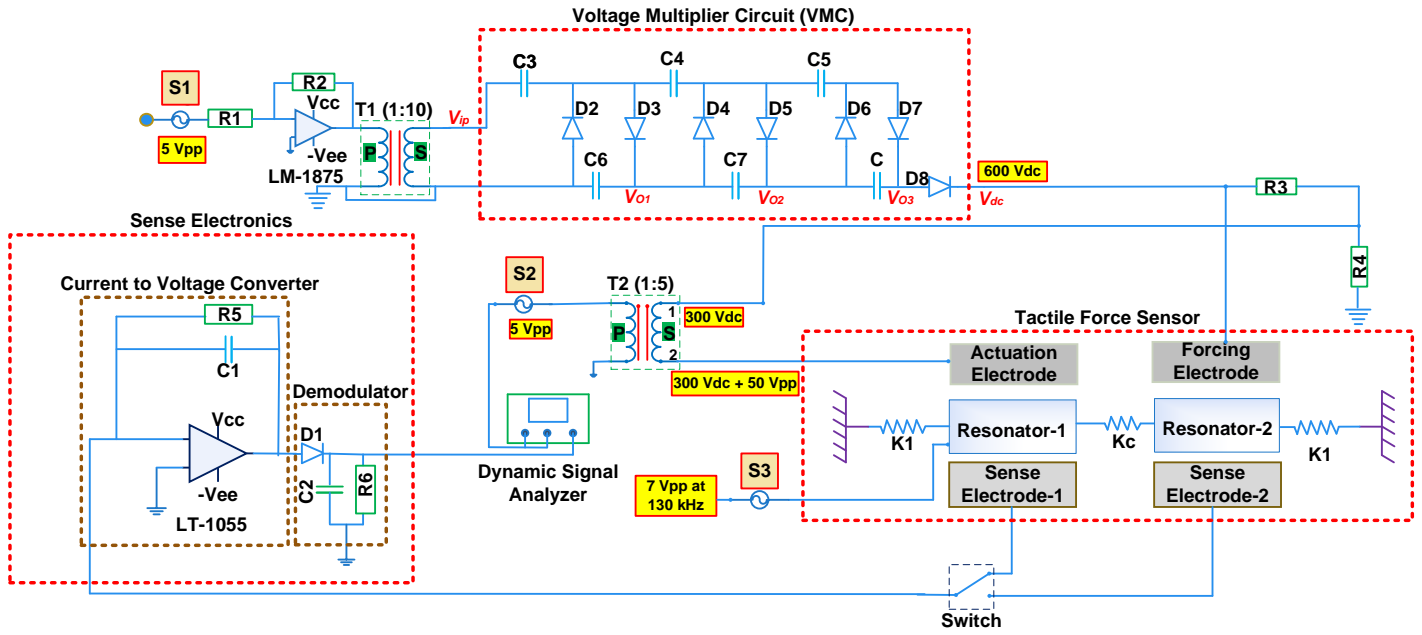


Fig. 10. Schematic diagram of the electronics circuit for the actuation and oscillation amplitude sensing of the 2-DOF WCRs in the tactile force sensor.

sensing electronics circuit. The actuation electronics circuit provides DC voltage to both forcing electrode, and actuation electrode. The actuation electronics circuit consists of a voltage multiplier circuit (VMC) which rectifies a sinusoidal signal labeled as S1 in the schematic and acts as voltage doubler. The signal (S1) is amplified and fed into the primary coil of step-up transformer T1. The output of T1 is then rectified and multiplied by a 3-stage (VMC). Each stage of VMC consists of voltage doubler connected in cascaded form. The voltage doubler multiplies the input AC voltage (V_{ip}) with the factor of 2 ($V_{O1} = V_{O2} = V_{O3} = 2 \times V_{ip}$), Where, V_{O1}, V_{O2}, V_{O3} , are output voltages of stage-1, stage-2, and stage-3 respectively. The output voltage of each stage of VMC are added and ideally, the resultant output voltage is 6 times higher than the input AC ($V_{dc} = V_{O1} + V_{O2} + V_{O3} = 6 \times V_{ip}$). The output signal of voltage multiplier is divided by a voltage divider consisting of resistor R3 and R4, which divides V_{dc} by a factor of 2. The output V_o from the VMC is connected to the forcing electrode and the divided voltage is connected to the terminal 1 of transformer (T2) at secondary side (S) for superimposition of AC and DC.

The electronics developed for the tactile force sensor is for open loop measurement. In open loop measurement, an AC sweep signal labeled as S2 is generated from the DSA which is connected to the primary side (P) of T2. Signal S2 is 5 Vpp with varying frequency ranging from 16 Hz to 30 Hz. The signal (S2) is stepped up and superimposed on V_{dc} at secondary terminal 2 of transformer (T2). The DC voltage (V_{dc}) can be adjusted by changing the resistor (R2) from the inverting amplifier or changing the amplitude of S1, while amplitude of AC actuation voltage can be controlled from the DSA.

The oscillation amplitude of 2-DOF WCRs is sensed through a capacitive sensing mechanism. A high frequency signal (S3) of 130 kHz is applied to the WCRs. When a resonator moves from the initial position, capacitance between the sensing electrode and resonator changes. This capacitance

change is modulated on the applied signal S3, which is converted to voltage using a gain resistor (R5) of 1.5 M Ω . The junction field effect transistor input based amplifier (LT-1055) is used to convert the current signal into voltage. The modulated signal is then demodulated by using a combination of schottky diode (D1), resistor (R6), and capacitor (C2). A switch is employed to measure the oscillation of each resonator.

5. Results and Discussion

The harmonic response of the tactile force sensor is first characterized by varying the V_{DC} to the resonator 1 in the 2-DOF WCRs system, when external force was not present. The DC voltage is varied from 0 V to 300 V, and amplitude of AC voltage is set at 50V_p. Figure 11(a) and 11(b) shows the oscillation amplitudes and resonant frequency of both resonators with increasing DC voltage. The oscillation amplitudes of both resonators increase with an increase in the bias voltage to the resonator 1. The high oscillation amplitude of resonators results in a higher effective signal to noise ratio due to the increased strength of electromechanical transduction.

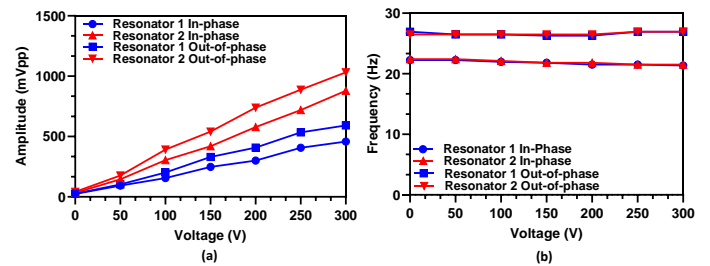


Fig. 11. Effect of increasing DC bias voltage on the, (a) oscillation amplitudes, and (b) resonant frequency of the 2-DOF WCRs.

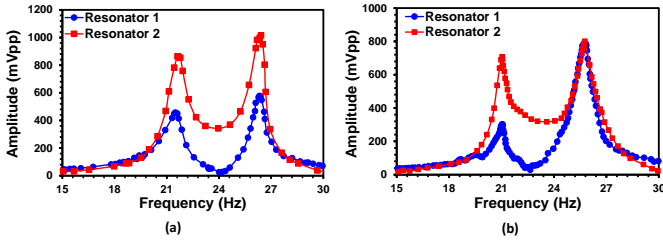


Fig. 12. Frequency response of the 2-DOF WCRs. (a) when no external force is applied. (b) with an applied force.

The results show that at low value of the DC actuation voltages, the AR for the two resonators is close to one at both modes. However, with an increase in the DC actuation voltage the AR decreases at both modes. The higher oscillation amplitude of resonator 2 can be observed due to the initial mechanical structural irregularity. The AR of 0.53 and 0.52 is observed for in-phase and out-of-phase mode respectively at 300 V. Figure 11(b) shows the resonant frequency of WCRs with increasing biasing voltage. The resonant frequency of both resonators is same and frequency shift of 0.84 Hz, and 0.47 Hz is obtained for in-phase and out-of-phase mode respectively for a 0-300 V range.

The frequency response of sensor is acquired by actuating the resonator 1 at 300V DC and 50V AC. The forcing cantilever is applied 600V DC for the stiffness perturbation. Figure 12(a) shows the frequency response of both resonator 1 and resonator 2 with no external perturbation. The sensor output is presented in the form of output voltage, which is processed using the sensing electronics. The resonant frequency for the first two modes is observed at 21.65 Hz and 26.37 Hz respectively with Δf of 4.72 Hz. The measured Δf is nearly twice the $2\Delta f_{3dB}$ value, which is 1.8 Hz, thus satisfying the mode-aliasing condition. The oscillation amplitude of resonator 2 is higher in comparison to the resonator 1 at both modes of operation. The higher amplitude of resonator 2 can be attributed to the presence of the actuation electrode part. As shown in Fig. 9(a), the top area of resonator 2 remains open for forcing cantilever, whereas top area of resonator 1 is covered by the actuation electrode. Consequently, resonator 1 experiences two parallel walled surfaces, increasing the overall air damping effect on resonator 1. This leads to the higher rate of increase in amplitude of resonator 2 with the increasing actuation voltages. The AR value for the resonators at first and second mode is 0.53 and 0.52 respectively. Figure 12 (b) shows frequency response of the 2-DOF WCRs with an applied input force of 20 mN. The frequency of WCRs shifts from 21.65 Hz to 20.9 Hz at first mode and 26.37 Hz to 25.7 Hz at second mode.

The oscillation amplitude of resonator 1 at first mode is 302 mV_{pp}, which is lower than the unperturbed value of 450 mV_{pp}. The oscillation amplitude at second mode for the resonator 1 is 810 mV_{pp} which is higher than the unperturbed value of 547 mV_{pp}. In comparison to the resonator 1, the oscillation amplitudes of resonator 2 at both modes decreases to 708 mV_{pp} and 790 mV_{pp} respectively with respect to initial unperturbed values of 855 mV_{pp} and 1030 mV_{pp}. The experimentally observed force perturbation response of the 2-DOF WCRs is in good agreement with the numerical response

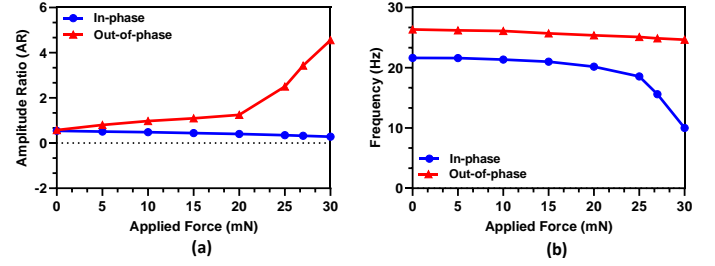


Fig. 13. Effect of increase in the applied force on (a) AR, and (b) resonant frequency of the 2-DOF WCRs at both the in-phase and out-of-phase mode.

showing that the negative stiffness perturbation, due to an applied force, increases the amplitude of resonator 1 at second mode and decreases it at first mode, whereas the amplitude of resonator 2 decreases at both modes.

The AR and frequency shift of the 2-DOF WCRs in the tactile force sensor with increasing applied force up to 30 mN is shown in Fig. 13. The AR at out-of-phase mode rises with an increase in applied force since the oscillation amplitude of resonator 1 increases and resonator 2 decreases at this mode. The AR increases rapidly above 20 mN due to the nonlinear relation of stiffness perturbation and applied force. The increase in the AR at out-of-phase mode is linear for 0-20 mN range with a coefficient of determination (R^2) value of 0.987. The absolute value of AR based sensitivity for the proposed tactile force sensor is calculated to be 0.0338 which gives relative AR sensitivity $[(AR^{20mN} - AR^{0mN})/AR^{20mN} \times 10^6]$ value of 27040 ppm/mN. The absolute and relative AR sensitivity at in-phase mode of the tactile sensor is 0.00866 and 24074 ppm/mN respectively. The results reveal that the sensor can be operated at out-of-phase mode for better sensitivity. The resonant frequency shift of WCRs is shown in Fig 13(b). The frequency shift is higher at in-phase mode with an applied force. The frequency of WCRs shifts from 21.65 Hz to 20.9 Hz for 20 mN range. The relative frequency based sensitivity of the sensor is calculated to be 3553 ppm/mN and 1839 ppm/mN at first and second mode respectively.

The resolution of the tactile force sensor is minimum detectable signal which is bounded by the oscillation amplitude noise fluctuation and sensitivity. Thermomechanical noise is the primary source of noise in 3dB bandwidth of system, which is caused by the dynamic equilibrium between the mechanical energy of resonators and surrounding thermal energy. Assuming a Gaussian noise for the system and $\Delta\omega_{3dB} \ll \omega_r$, the noise equivalent displacement of resonators in terms of amplitude noise fluctuations can be expressed as [23];

$$x_r^{noise} = \sqrt{\frac{4k_b T \Delta\omega_{3dB} Q}{m_r \omega_r^3}} \quad (22)$$

where T , k_b , m_r , ω_r , and Q is the ambient temperature, Boltzmann constant, resonator mass, resonant frequency, and quality factor respectively. The minimum resolvable shift in stiffness of the resonator 2 due to the input force perturbation can be estimated by using the following expression [23];

$$\left(\frac{\Delta k}{k}\right)_{min} = 8 \frac{k_c}{k} \sqrt{\frac{k_b T \Delta\omega_{3dB}}{2m_r \omega_r^2 x_r^2 Q}} \quad (23)$$

The force resolution for the proposed tactile sensor can

be acquired using the minimum stiffness change divided by the sensitivity of the sensor;

$$Resolution = \frac{(\Delta k/k)_{min}}{sensitivity} = 0.53 \mu\text{N} \quad (24)$$

The resolution measured in equation (25) considers only the thermomechanical noise. However, the force resolution based on fluctuation amplitude noise is calculated by measuring the response of resonator without applying the DC voltage [38]. The dynamic frequency response of resonator 1 is observed on DSA and AC signal is fixed at 50 Vp. The standard deviation for the lower fluctuation is calculated as minimum amplitude x_2 , while the highest peak of the resonators at normal operating point is x_1 . Therefore, the resolution of the sensor based on amplitude fluctuation noise is calculated as,

$$AR \text{ Resolution} = \frac{\left(\frac{x_2}{x_1}\right)_{min}}{Sensitivity} = 7.3 \mu\text{N} \quad (26)$$

The tactile force sensor performance is observed under varying temperature conditions. The sensor is placed inside the acrylic chamber and temperature of chamber is varied from 20°C-65°C using heat-gun as shown in Fig. 14(a). The time domain response of the sensor for the varying temperature, shown in Fig. 14(c), indicates that the varying temperature has a negligible effect on the response of resonators. The sensor is also subjected to external vibrations using a shaker to observe the effect of vibrations in the range of human hand tremor frequency as shown in Fig. 14(b). The actuation voltages (both AC and DC) of the resonators are set to 0, while time-domain response is calculated in the range of 4 Hz-12 Hz of external excitation frequency. The response of the sensor to varying excitation frequencies, as shown in Fig. 14(d), suggests that the sensor can perform adequately in a low frequency vibrational environment.

The comparison of FEM based simulations and experimental results for the 2-DOF WCRs in the proposed tactile force sensor under an input force range of 20 mN are shown in Table. II. The results show that AR sensitivity at mode

TABLE II: COMPARISON OF THE MODE FREQUENCIES, AR, AR SENSITIVITY, AND FREQUENCY SENSITIVITY, OF SIMULATED AND EXPERIMENTAL RESULTS FOR THE 2-DOF WCRS BASED TACTILE FORCE SENSOR.

Parameter	FEM simulation	Experimental
Force range	0-20 mN	0-20 mN
Amplitude ratio (AR)	Mode 1	1.012
	Mode 2	0.99
Resonant frequency	Mode 1	20.65 Hz
	Mode 2	23.9 Hz
AR sensitivity (ppm/mN)	Mode 1	30769
	Mode 2	35000
Frequency sensitivity (ppm/mN)	Mode 1	4656.8
	Mode 2	2301.2

2 is higher than mode 1 for simulated as well as for the experimental results. Moreover, the AR sensitivity for both Mode 1 and mode 2 is higher than the frequency based sensitivity. The experimental AR based sensitivity is 8 times higher than the frequency based sensitivity.

Table. III shows the comparison of the proposed mode-localization based tactile force sensor with the state-of-the-art tactile force sensor presented in the literature and commercially available tactile force sensor that operate on different transduction principle. The proposed mode-localization based tactile force sensor shows lower cost and higher resolution in comparison to the other tactile force sensors.

The design of the sensor is very simple, and sensor can be easily integrated into minimally invasive robotic surgery (MIRS) based applications for low-cost solution by tailoring the size and shape of the sensor. The piezoelectric resonance tactile sensors are reported to be used for detecting the hardness of soft tissue for lump-localization and tumor detection. The developed mode-localization based tactile sensors can also be incorporated in these applications by using the normal force contact. The research on tactile sensors in which to measure the forces at points distributed in multiple points are tactile sensing arrays. These tactile sensing arrays are designed to mimic the fingertip sense of touch of the human body. The spatial acuity of mechanoreceptors at fingertip of human is 1mm and it's up to 30mm for human belly. In mode-localization based tactile sensors, multiple coupled resonator array design of tactile sensor with ultra-high sensitivity can be developed to mimic the

TABLE III: COMPARISON OF THE MODE LOCALIZATION BASED TACTILE FORCE SENSOR WITH THE STATE-OF-THE-ART TACTILE SENSORS IN THE LITERATURE.

Author	Working Principle	Range	Resolution	Sensitivity	Cost (\$)
Li et al. [15]	Piezoresistive	3 N	0.15 N	-	-
Liu et al. [10]	Optical	6 mN	0.25 mN	40 nm/mN	-
Naidu et al. [34]	Capacitive	0.6 N	4 mN	1 pF/N	35
Li et al. [8]	FBG	0-5 N	0.93 mN	1014 pm/N	-
Arshad et al. [7]	Fringing Electric field	0-5 N	4.3 mN	0.0378/ N	26
Nano17 [38]	Strain gauge	17 N	3 mN	-	5500
Honeywell-FSS [39]	Piezoresistive	5N	variable	7.2 mV/N	120
This Work	Mode-localization	20 mN	7.3 μN	27040 ppm/mN	20

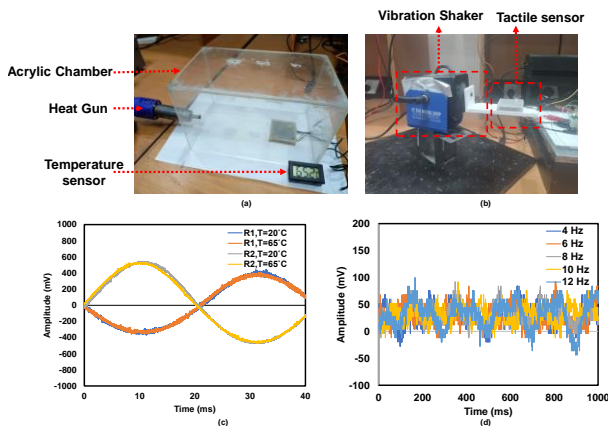


Fig. 14. Effect of environmental factors on the performance of tactile force sensor (a) Experimental setup for temperature variation. (b) experimental setup for the application of external vibration. (c) A time domain graph of WCRs with different temperature values at out-of-phase mode. (d) A time-domain graph showing vibration measurements of a resonator subjected to varying frequency of excitation vibrations within the range of human hand tremor frequencies.

human receptors. In the developed tactile force sensor, the measurements of the sensor are done with the open-loop characterization. The modeling of dynamic perturbation system and closed-loop characterization of the mode-localization sensor will enable its use in dynamic force applications.

6. Conclusion

A single point contact mesoscale tactile force sensor design based on the mode-localization effect in 2-DOF WCRs is fabricated and tested to attain high force resolution. The AR and resonant frequency of the WCRs is discussed as an output parameter to measure the input force. The external perturbation versus AR and frequency shift graph for negative stiffness perturbation showed higher AR at second mode and higher frequency shift at first mode. The first two operating modes of the sensor are in-phase and out-of-phase mode of vibration. The two modes are experimentally obtained at 21.65 Hz and 26.37 Hz at 0 mN force. The relative AR based sensitivity at out-of-phase mode is 27040 ppm/mN which is higher than the in-phase mode sensitivity of 24074 ppm/mN for 20 mN force range. The sensitivity based on AR is 8 times higher, compared to the frequency based sensitivity. The experimentally calculated resolution of the tactile force sensor is 7.3 μ N. The sensor has shown a very high resolution compared to the state-of-the-art tactile force sensors presented in the literature. The sensor performance can be further enhanced in-terms of sensitivity and range by using the multi-DoF WCRs as a tactile sensing array.

Acknowledgments

This work was supported by the Higher Education Commission (HEC), Pakistan and the British Council UK within the framework of the Innovative and Collaborative Research Partnerships Grants (ICRG) program under the project. No. ICRG-147.

References

- [1] Zemit, Nabil, Guillaume Morel, Tobias Ortmaier, and Nicolas Bonnet. "Mechatronic Design of a New Robot for Force Control in Minimally Invasive Surgery." *IEEE/ASME Transactions on Mechatronics* 12, no. 2 (2007): 143–53. <https://doi.org/10.1109/TMECH.2007.892831>.
- [2] Kim, Uikyum, Dong Hyuk Lee, Yong Bum Kim, Dong Yeop Seok, Jinho So, and Hyouk Ryeol Choi. "S-Surge: Novel Portable Surgical Robot with Multi-axis Force-Sensing Capability for Minimally Invasive Surgery." *IEEE/ASME Transactions on Mechatronics* 22, no. 4 (2017). <https://doi.org/10.1109/TMECH.2017.2696965>.
- [3] Yeh, Sheng Kai, Meng Lin Hsieh, and Weileun Fang. "CMOS-Based Tactile Force Sensor: A Review." *IEEE Sensors Journal*, 2021. <https://doi.org/10.1109/JSEN.2021.3060539>.
- [4] Luo, Shan, Joao Bimbo, Ravinder Dahiya, and Hongbin Liu. "Robotic Tactile Perception of Object Properties: A Review." *Mechatronics*, 2017. <https://doi.org/10.1016/j.mechatronics.2017.11.002>.
- [5] Chuang, Cheng Hsin, Tsan Hsiu Li, I. Chinms Chou, and Ying Juimr Teng. "Piezoelectric Tactile Sensor for Submucosal Tumor Detection in Endoscopy." *Sensors and Actuators, A: Physical* 244 (2016): 299–309. <https://doi.org/10.1016/j.sna.2016.04.020>.
- [6] Hooshiar, Amir, Alireza Payami, Javad Dargahi, and Siamak Najarian. "Magnetostriction-Based Force Feedback for Robot-Assisted Cardiovascular Surgery Using Smart Magnetorheological Elastomers." *Mechanical Systems and Signal Processing* 161 (2021): 107918. <https://doi.org/10.1016/j.ymssp.2021.107918>.
- [7] Arshad, Adeel, Muhammad Mubasher Saleem, Mohsin Islam Tiwana, Hamood ur Rahman, Sohail Iqbal, and Rebecca Cheung. "A High Sensitivity and Multi-Axis Fringing Electric Field Based Capacitive Tactile Force Sensor for Robot Assisted Surgery." *Sensors and Actuators A: Physical* 354 (2023): 114272. <https://doi.org/https://doi.org/10.1016/j.sna.2023.114272>.
- [8] Li, Tianliang, Chaoyang Shi, and Hongliang Ren. "A High-Sensitivity Tactile Sensor Array Based on Fiber Bragg Grating Sensing for Tissue Palpation in Minimally Invasive Surgery." *IEEE/ASME Transactions on Mechatronics* 23, no. 5 (2018): 2306–15. <https://doi.org/10.1109/TMECH.2018.2856897>.
- [9] Yip, Michael C., Shelten G. Yuen, and Robert D. Howe. "A Robust Uniaxial Force Sensor for Minimally Invasive Surgery." *IEEE Transactions on Biomedical Engineering* 57, no. 5 (2010): 1008–11. <https://doi.org/10.1109/TBME.2009.2039570>.
- [10] Liu, Xuan, Iulian I. Iordachita, Xingchi He, Russell H. Taylor, and Jin U. Kang. "Miniature Fiber-Optic Force Sensor Based on Low-Coherence Fabry-Pérot Interferometry for Vitreoretinal Microsurgery." *Biomedical Optics Express* 3, no. 5 (2012): 1062. <https://doi.org/10.1364/boe.3.001062>.
- [11] Tiwana, Mohsin I., Stephen J. Redmond, and Nigel H. Lovell. "A Review of Tactile Sensing Technologies with Applications in Biomedical Engineering." *Sensors and Actuators, A: Physical* 179 (2012): 17–31. <https://doi.org/10.1016/j.sna.2012.02.051>.
- [12] Puangmali, Pinyo, Hongbin Liu, Lakmal D. Seneviratne, Prokar Dasgupta, and Kaspar Althoefer. "Miniature 3-Axis Distal Force Sensor for Minimally Invasive Surgical Palpation." *IEEE/ASME Transactions on Mechatronics* 17, no. 4 (2012): 646–56. <https://doi.org/10.1109/TMECH.2011.2116033>.
- [13] Kim, Uikyum, Yong Bum Kim, Dong Yeop Seok, Jinho So, and Hyouk Ryeol Choi. "A Surgical Palpation Probe with 6-Axis Force/Torque Sensing Capability for Minimally Invasive Surgery." *IEEE Transactions on Industrial Electronics* 65, no. 3 (2018): 2755–65. <https://doi.org/10.1109/TIE.2017.2739681>.
- [14] Wisitsoraat, A., V. Patthanasetakul, T. Lomas, and A. Tuantranont. "Low Cost Thin Film Based Piezoresistive MEMS Tactile Sensor." *Sensors and Actuators, A: Physical* 139, no. 1-2 SPEC. ISS. (2007): 17–22. <https://doi.org/10.1016/j.sna.2006.10.037>.
- [15] Li, Kun, Bo Pan, Juncheng Zhan, Wenpeng Gao, Yili Fu, and Shuguo Wang. "Design and Performance Evaluation of a 3-Axis Force Sensor for MIS Palpation." *Sensor Review* 35, no. 2 (2015): 219–28. <https://doi.org/10.1108/SR-04-2014-632>.
- [16] Rehan, Muhammad, Muhammad Mubasher Saleem, Mohsin Islam Tiwana, Rana Iqtidar Shakoor, and Rebecca Cheung. "A Soft Multi-Axis High Force Range Magnetic Tactile Sensor for Force Feedback in Robotic Surgical Systems." *Sensors* 22, no. 9 (2022): 1–17. <https://doi.org/10.3390/s22093500>.
- [17] Wang, Hongbo, Junwai Kow, Nicholas Raske, Gregory de Boer, Mazdak Ghajari, Robert Hewson, Ali Alazmani, and Peter Culmer. "Robust and High-Performance Soft Inductive Tactile Sensors Based on the Eddy-Current Effect." *Sensors and Actuators, A: Physical* 271 (2018): 44–52. <https://doi.org/10.1016/j.sna.2017.12.060>.
- [18] Bandari, Naghme, Javad Dargahi, and Muthukumaran Packirisamy. "Tactile Sensors for Minimally Invasive Surgery: A Review of the State-of-the-Art, Applications, and Perspectives." *IEEE Access*, 2020. <https://doi.org/10.1109/ACCESS.2019.2962636>.
- [19] Yun, Yahui, Yaming Wang, Hao Guo, Yaoyao Wang, Hongtao Wu, Bai Chen, and Feng Ju. "A Resonant Tactile Stiffness Sensor for Lump Localization in Robot-Assisted Minimally Invasive Surgery." *Proceedings of the Institution of Mechanical Engineers, Part H: Journal of Engineering in Medicine* 233, no. 9 (2019): 909–20. <https://doi.org/10.1177/0954411919856519>.
- [20] Oliva Uribe, David, Johan Schoukens, and Ralf Stroop. "Improved Tactile Resonance Sensor for Robotic Assisted Surgery." *Mechanical Systems and Signal Processing* 99 (2018): 600–610. <https://doi.org/10.1016/j.ymssp.2017.07.007>.
- [21] Dhar, Parag R., and Jean W. Zu. "Design of a Resonator Device for in Vivo Measurement of Regional Tissue Viscoelasticity." *Sensors and Actuators, A: Physical* 133, no. 1 (2007): 45–54. <https://doi.org/10.1016/j.sna.2006.03.030>.
- [22] Zhang, Lei, Feng Ju, Yanfei Cao, Yaoyao Wang, and Bai Chen. "A Tactile Sensor for Measuring Hardness of Soft Tissue with Applications to Minimally Invasive Surgery." *Sensors and Actuators, A: Physical* 266 (2017): 197–204. <https://doi.org/10.1016/j.sna.2017.09.012>.
- [23] Saleem, Muhammad Mubasher, Shayaan Saghri, Syed Ali Raza Bukhari, Amir Hamza, Rana Iqtidar Shakoor, and Shafaat Ahmed Bazaz. "A Low-g MEMS Accelerometer with High Sensitivity, Low

- Nonlinearity and Large Dynamic Range Based on Mode-Localization of 3-Dof weakly Coupled Resonators.” *Micromachines* 12, no. 3 (2021). <https://doi.org/10.3390/mi12030310>
- [24] Li, Han, Zhao Zhang, Luhan Zu, Yongcun Hao, and Honglong Chang. “Micromechanical Mode-Localized Electric Current Sensor.” *Microsystems & Nanoengineering* 8, no. 1 (2022): 42. <https://doi.org/10.1038/s41378-022-00375-1>.
- [25] Bukhari, Syed Ali Raza, Muhammad Mubasher Saleem, Amir Hamza, and Shafaat Ahmed Bazaz. “A Novel Design of High Resolution MEMS Gyroscope Using Mode-Localization in Weakly Coupled Resonators.” *IEEE Access* 9 (2021): 157597–608. <https://doi.org/10.1109/ACCESS.2021.3123152>.
- [26] Zhao, Chun, Graham S. Wood, Jianbing Xie, Honglong Chang, Suan Hui Pu, and Michael Kraft. “A Force Sensor Based on Three Weakly Coupled Resonators with Ultrahigh Sensitivity.” *Sensors and Actuators, A: Physical* 232 (2015): 151–62. <https://doi.org/10.1016/j.sna.2015.05.011>.
- [27] Lyu, Ming, Jian Zhao, Najib Kacem, Bin Tang, Pengbo Liu, Jiahao Song, Heng Zhong, and Yu Huang. “Computational Investigation of High-Order Mode Localization in Electrostatically Coupled Microbeams with Distributed Electrodes for High Sensitivity Mass Sensing.” *Mechanical Systems and Signal Processing* 158 (2021): 107781. <https://doi.org/10.1016/j.ymsp.2021.107781>.
- [28] Guo, Xin, Bo Yang, and Cheng Li. “Design, Modeling and Theoretical Analysis of a Novel Dual-Axis Hair Flow Sensor Based on Mode Localization of Weakly Coupled Resonators.” *AIP Advances* 9, no. 5 (2019). <https://doi.org/10.1063/1.5099160>.
- [29] Zhang, Hemin, Jie Huang, Weizheng Yuan, and Honglong Chang. “A High-Sensitivity Micromechanical Electrometer Based on Mode Localization of Two Degree-of-Freedom Weakly Coupled Resonators.” *Journal of Microelectromechanical Systems* 25, no. 5 (2016): 937–46. <https://doi.org/10.1109/JMEMS.2016.2598780>.
- [30] Zhang, Hemin, Jing Yang, Weizheng Yuan, and Honglong Chang. “Linear Sensing for Mode-Localized Sensors.” *Sensors and Actuators, A: Physical* 277 (2018): 35–42. <https://doi.org/10.1016/j.sna.2018.05.006>.
- [31] Humbert, Claude, Vincent Walter, and Thérèse Leblois. “A Mass Sensor Based on Digitally Coupled and Balanced Quartz Resonators Using Mode Localization.” *Sensors and Actuators A: Physical* 335 (2022). <https://doi.org/10.1016/j.sna.2022.113378>.
- [32] Rabenimanana, Toky, Vincent Walter, Najib Kacem, Patrice Le Moal, Gilles Bourbon, and Joseph Lardiès. “Mass Sensor Using Mode Localization in Two Weakly Coupled MEMS Cantilevers with Different Lengths: Design and Experimental Model Validation.” *Sensors and Actuators, A: Physical* 295 (2019): 643–52. <https://doi.org/10.1016/j.sna.2019.06.004>.
- [33] Judy, J. W. “Microelectromechanical Systems (MEMS): Fabrication, Design and Applications.” *Smart Materials and Structures* 10, no. 6 (2001): 1115–34. <https://doi.org/10.1088/0964-1726/10/6/301>.
- [34] Naidu, Anish S., Rajni V. Patel, and Michael D. Naish. “Low-Cost Disposable Tactile Sensors for Palpation in Minimally Invasive Surgery.” *IEEE/ASME Transactions on Mechatronics* 22, no. 1 (2017): 127–37. <https://doi.org/10.1109/TMECH.2016.2623743>.
- [35] “CRC Handbook of Chemistry and Physics, 84th Edition Edited by David R. Lide (National Institute of Standards and Technology). CRC Press LLC: Boca Raton. 2003. 2616 Pp. ISBN 0-8493-0484-9.” *Journal of the American Chemical Society* 126, no. 5 (2004): 1586–1586. <https://doi.org/10.1021/ja0336372>.
- [36] Liu, Man, and D. G. Gorman. “Formulation of Rayleigh Damping and Its Extensions.” *Computers and Structures* 57, no. 2 (1995). [https://doi.org/10.1016/0045-7949\(94\)00611-6](https://doi.org/10.1016/0045-7949(94)00611-6).
- [37] Riaz, Kashif, Shafaat A. Bazaz, M. Mubasher Saleem, and Rana I. Shakoor. “Design, Damping Estimation and Experimental Characterization of Decoupled 3-DoF Robust MEMS Gyroscope.” *Sensors and Actuators, A: Physical* 172, no. 2 (2011): 523–32. <https://doi.org/10.1016/j.sna.2011.09.032>.
- [38] Zhang, H., Li, B., Yuan, W., Kraft, M. & Chang, H. An Acceleration Sensing Method Based on the Mode Localization of Weakly Coupled Resonators. *J. Microelectromechanical Syst.* 25, 286–296 (2016).
- [39] ATI F/T Nano 17, Force Torque Sensor. Accessed: March 26, 2023. [Online]. Available: https://www.ati-ia.com/app_content/documents
- [40] Honeywell. FSS Series Low Profile Force Sensor. Accessed: March. 26, 2023. [Online]. Available: <https://sensing.honeywell.com/sensors/force-sensors/FSS-series>.